ChemSusChem

Supporting Information

Titanium Niobium Oxide $Ti_2Nb_{10}O_{29}$/Carbon Hybrid Electrodes Derived by Mechanochemically Synthesized Carbide for High-Performance Lithium-Ion Batteries

Öznil Budak, Pattarachai Srimuk, Mesut Aslan, Hwirim Shim, Lars Borchardt, and Volker Presser*

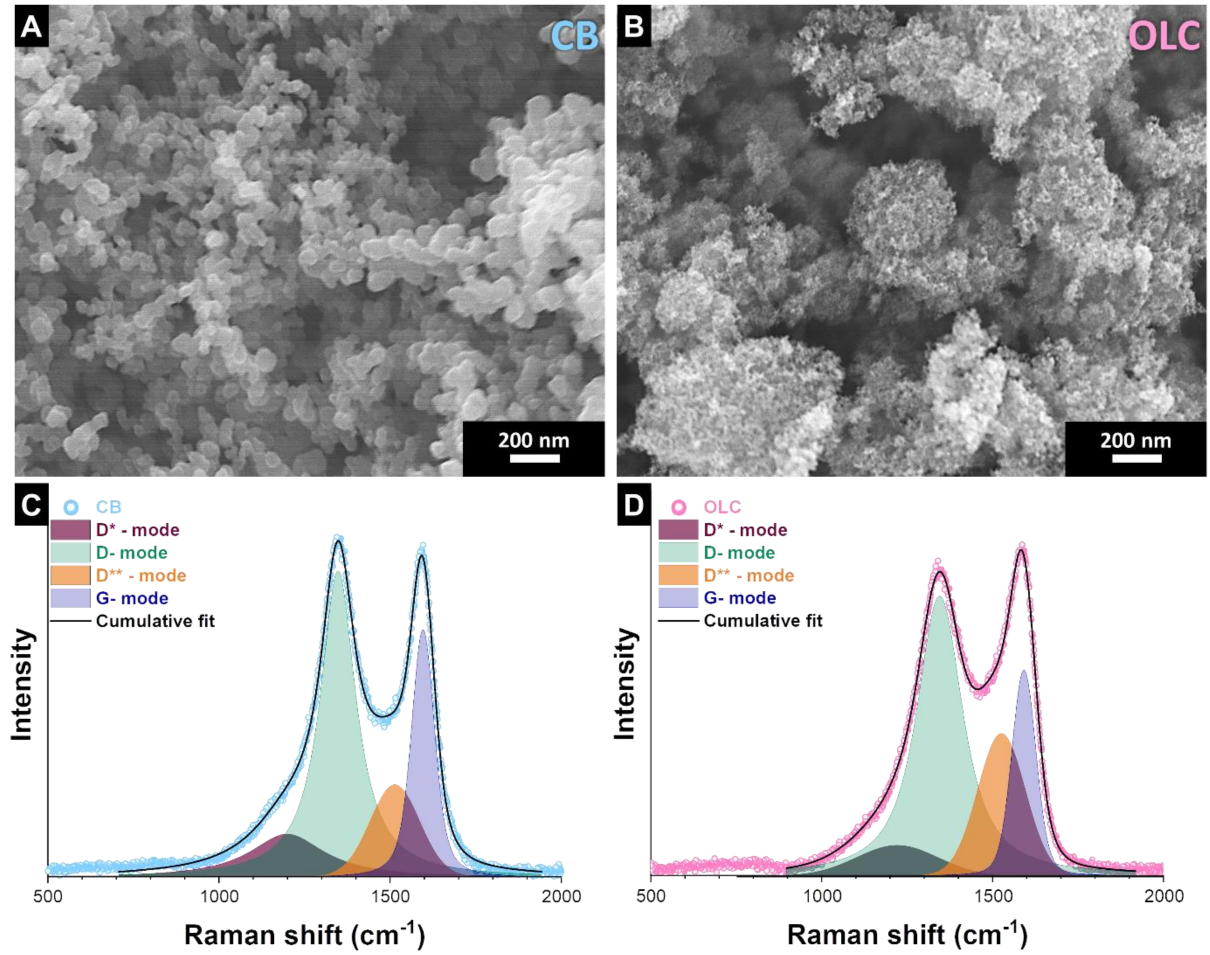

Fig. S1. (A-B) Scanning electron micrographs of (A) CB, and (B) OLC. Fitted Raman spectra of (C) CB, and (D) OLC.

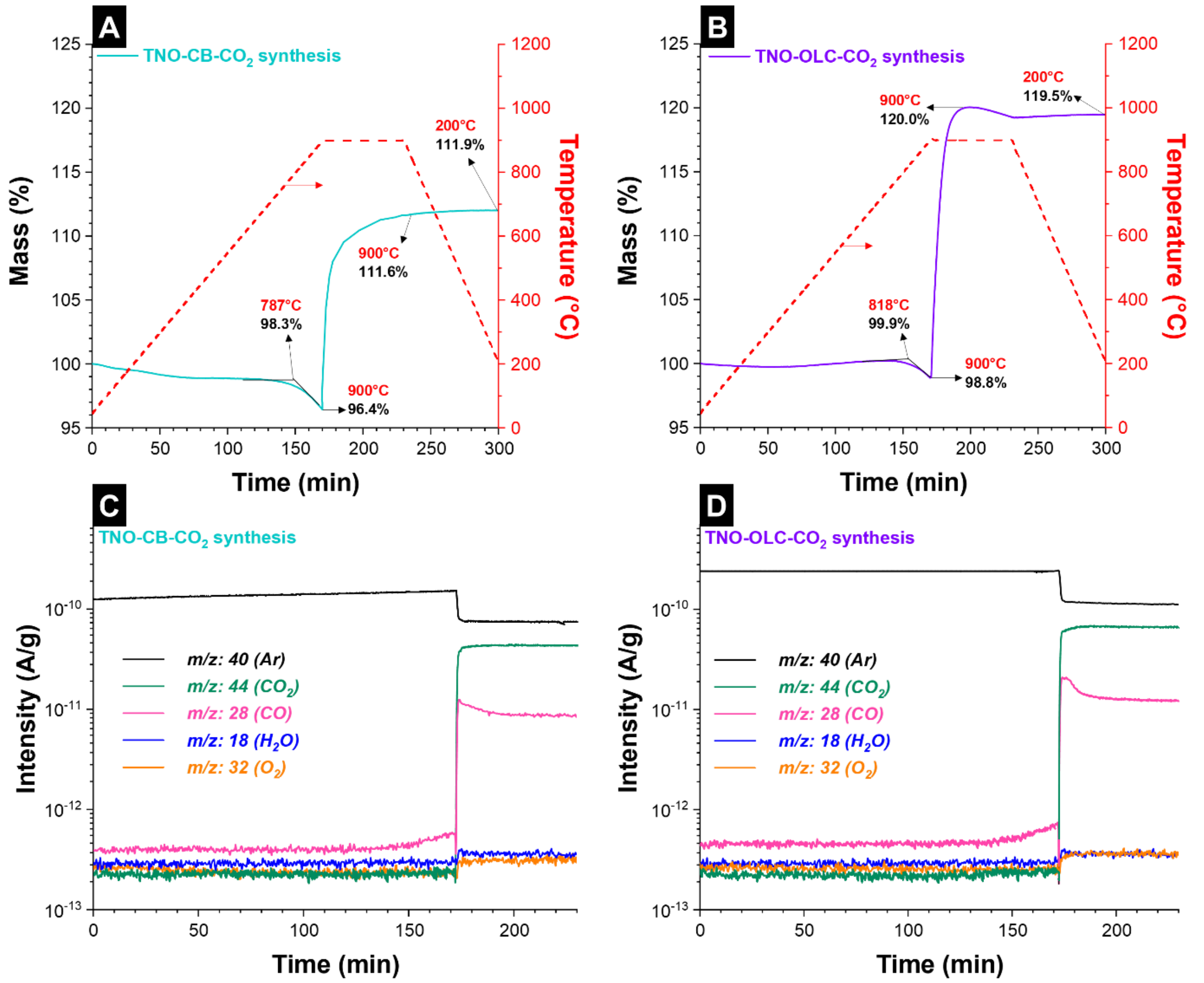

Fig. S2. (A-B) Thermograms of (A) TNO-CB-CO_2, and (B) TNO-OLC-CO_2 synthesis following the synthesis protocol of hybrid materials. The corresponding mass spectra of TGA-MS measurements of (C) TNO-CB-CO_2, and (D) TNO-OLC-CO_2 synthesis.

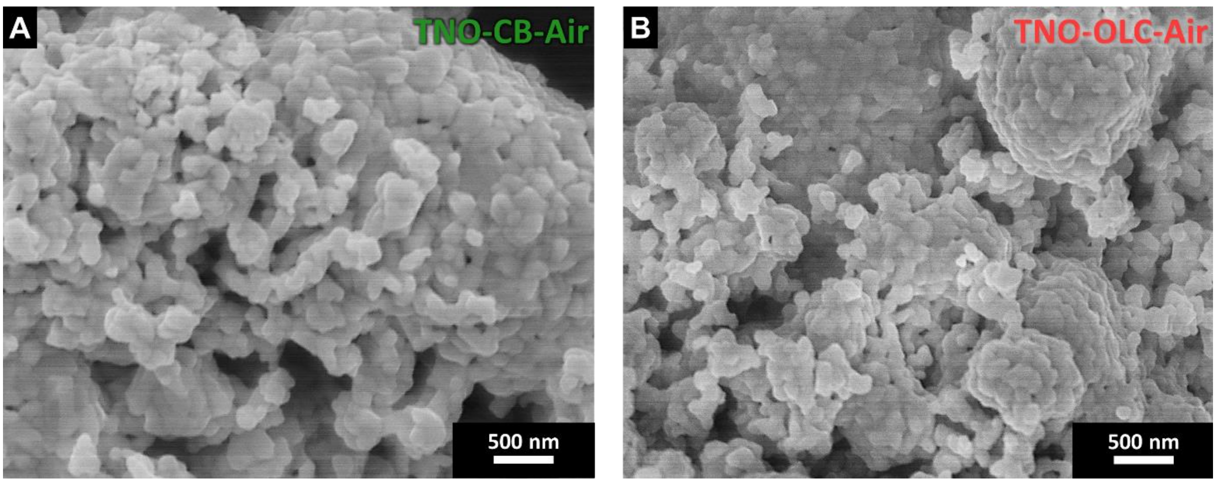

Fig. S3. (A-B) Scanning electron micrographs of (A) TNO-CB-Air, and (B) TNO-OLC-Air.

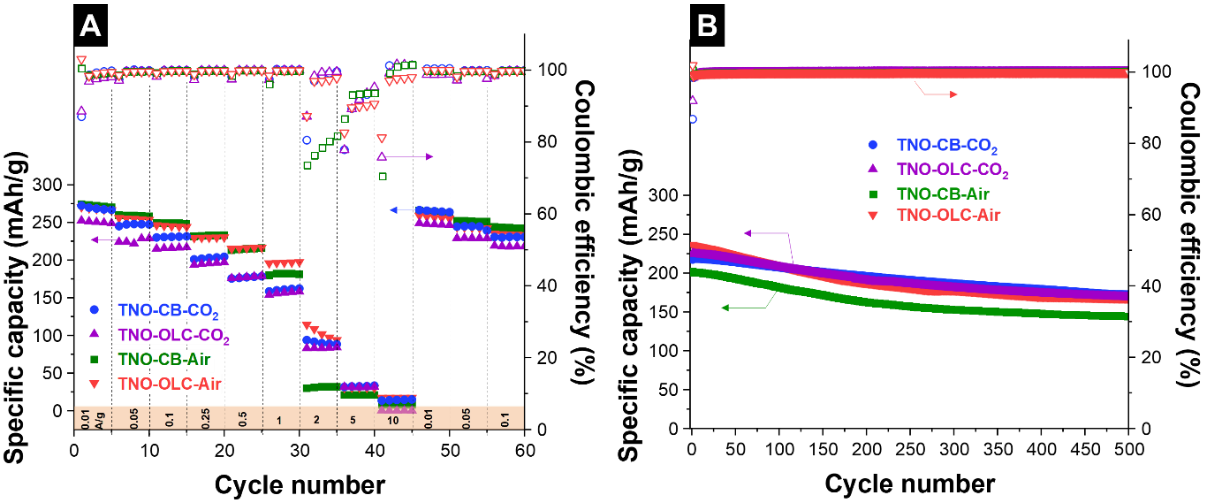

Fig. S4. (A) Rate handling performance of the hybrid and non-hybrid materials in the potential window of 1.0-2.5 V vs. Li/Li^+. (B) Cyclic stability performance of the hybrid and non-hybrid materials in the potential window of 1.0-2.5 V vs. Li/Li^+.

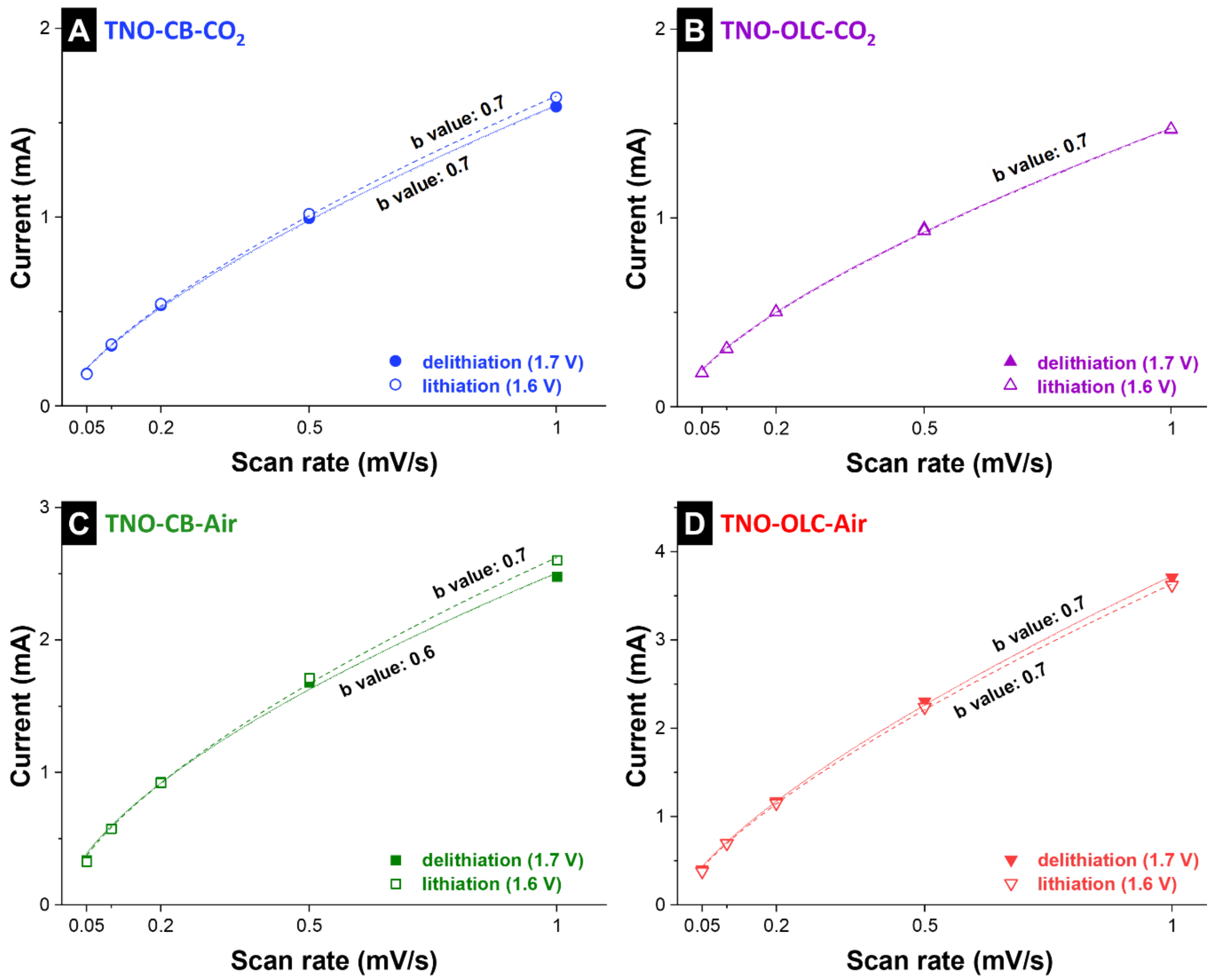

Fig. S5. Kinetic analysis of (A) TNO-CB-CO_2, (B) TNO-OLC-CO_2, (C) TNO-CB-Air, and (D) TNO-OLC-Air calculated from cyclic voltammograms at the different scan rates for the potential window of 1.0-2.5 V vs. Li/Li^+.

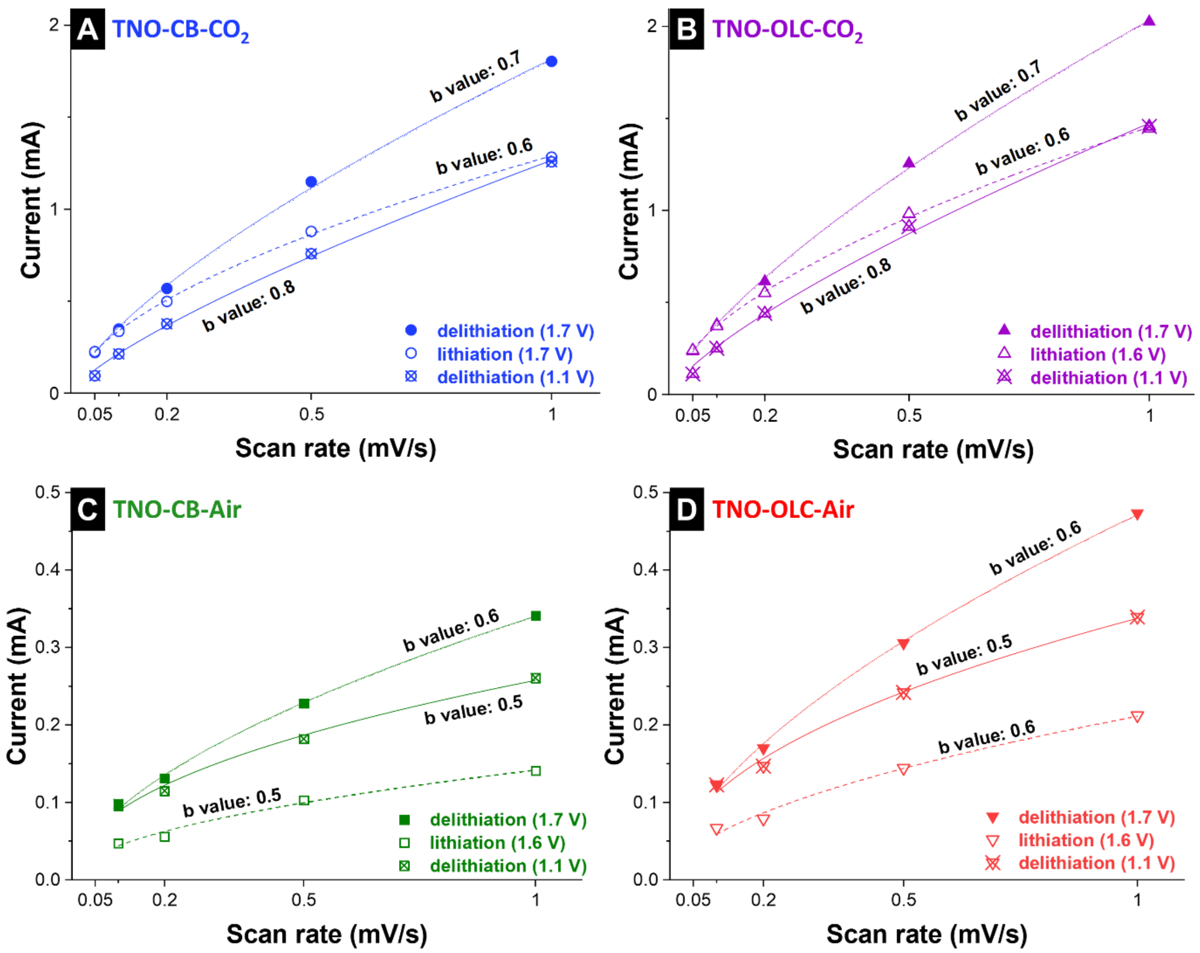

Fig. S6. Kinetic analysis of (A) TNO-CB-CO_2, (B) TNO-OLC-CO_2, (C) TNO-CB-Air, and (D) TNO-OLC-Air calculated from cyclic voltammograms at the different scan rates for the potential window of 0.05-2.5 V vs. Li/Li^+.

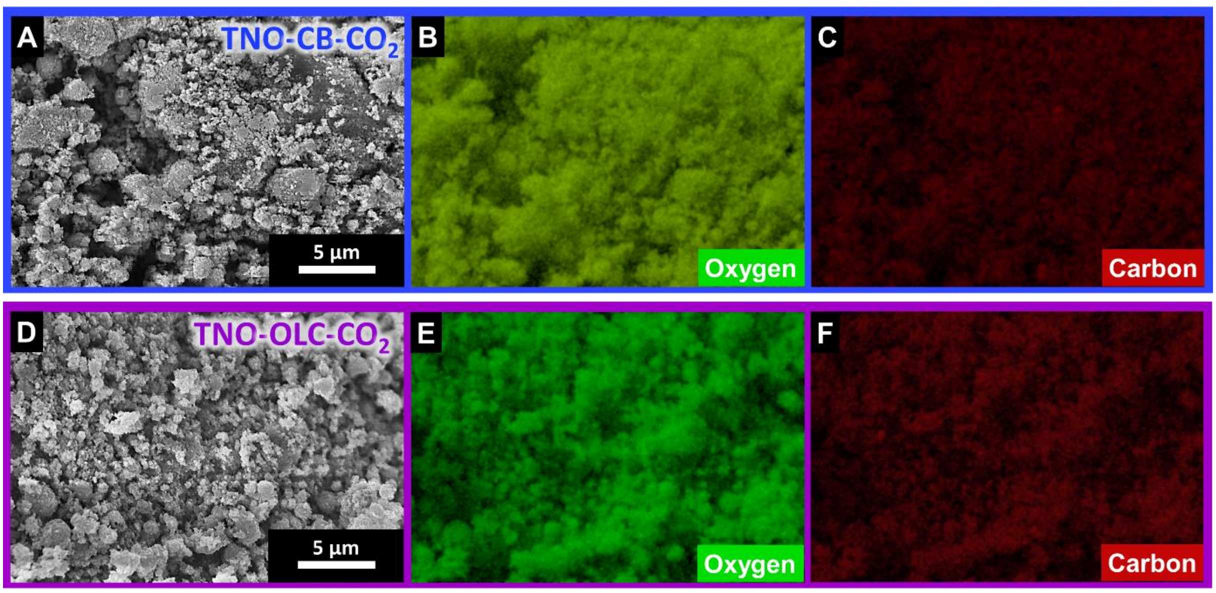

Fig. S7. (A-C) Analysis of the TNO-CB-CO_2 electrode: (A) Scanning electron micrographs, and (B-C) elemental mapping by EDX. (D-F) Analysis of the TNO-OLC-CO_2 electrode: (D) Scanning electron micrographs, and (E-F) elemental mapping by EDX.

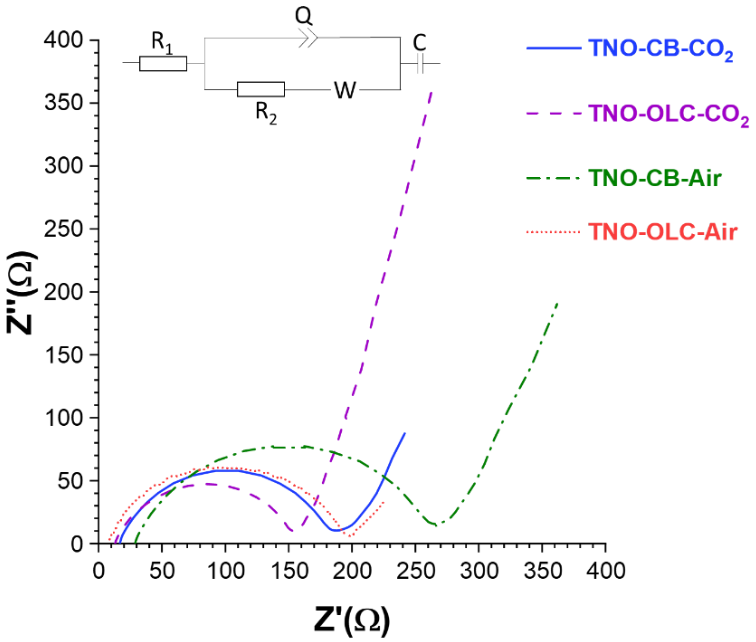

Fig. S8. Nyquist plot of hybrid and non-hybrid materials. The inset displays the equivalent circuit used for fitting of the electrochemical impedance spectra.

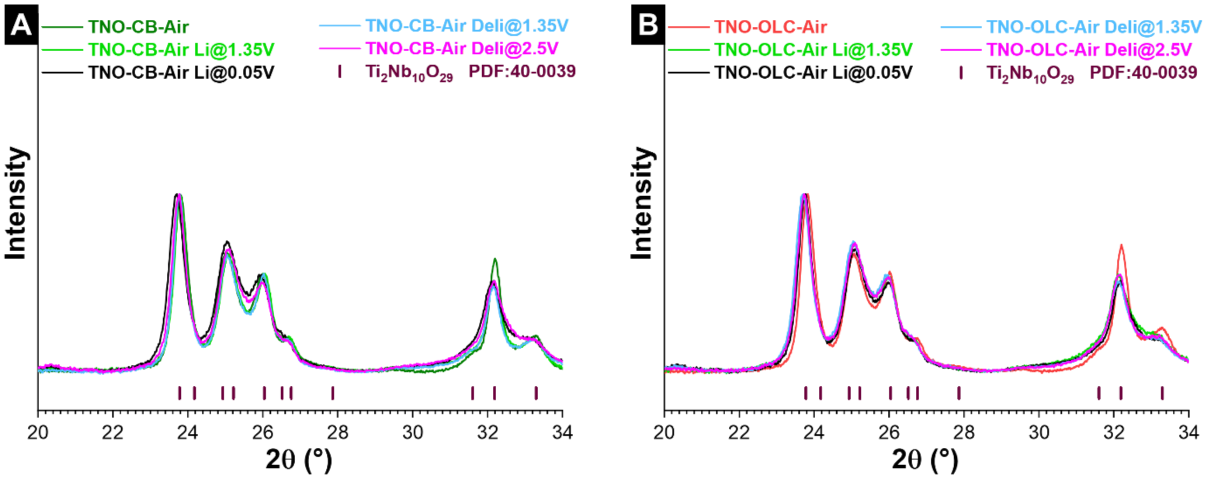

Fig. S9. X-ray diffraction patterns of (A) TNO-CB-Air, and (B) TNO-OLC-Air electrodes at the different lithiated/delithiated states (denoted as "Li" and "Deli").

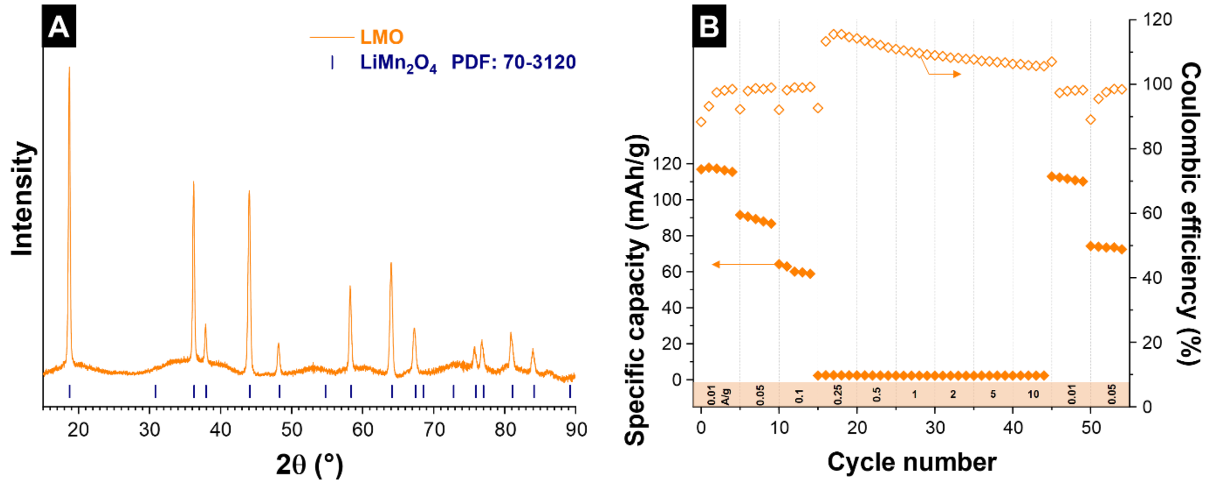

Fig. S10. (A) X-ray diffractogram of $LiMn_2O_4$ (LMO) with the reported Bragg positions from PDF 70-3120. (B) Rate handling performance of LMO.

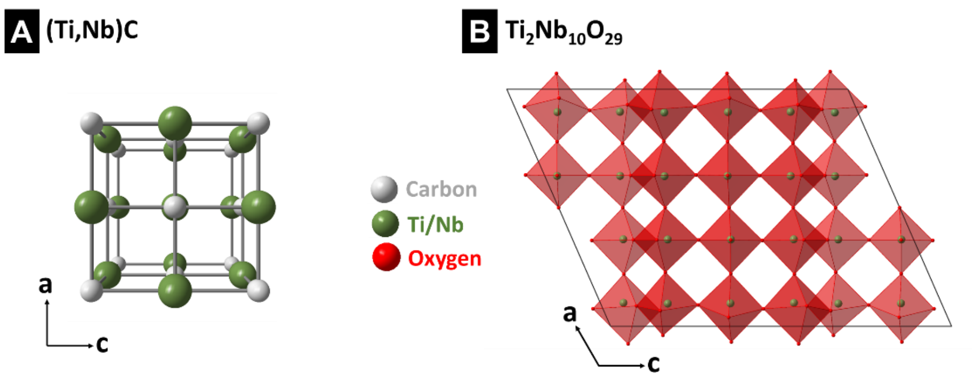

Fig. S11. Structural illustrations of the crystal lattice of (A) titanium niobium carbide (Ti,Nb)C, and (B) $Ti_2Nb_{10}O_{29}$.

Table S1. Rietveld refinement results of TNC-CB and TNC-OLC.

Sample	Phase	Space group	Lattice parameter (Å)	Volume ($Å^3$)	Domain size (nm)	Amount (mass%)	R_{wp} (%)
TNC-CB	(Ti,Nb)C	$Fm\bar{3}m$	*a* = 4.43(4)	87.09(4)	19.7(4)	98	2.3
	WC	$P\bar{6}m2$	*a* = 2.90(3) *c* = 2.85(3)	20.82(3)	>200	2	
TNC-OLC	(Ti,Nb)C	$Fm\bar{3}m$	*a* = 4.43(4)	88.12(4)	15.3(4)	98	2.5
	WC	$P\bar{6}m2$	*a* = 2.90(6) *c* = 2.85(6)	20.76(6)	>200	2	

Table S2. Le Bail analysis results of the analysis of X-ray diffraction patterns of TNO-CB-CO_2, TNO-OLC-CO_2, TNO-CB-Air, and TNO-OLC-Air.

Sample	Phase	Space group	Lattice parameter (Å)	Interaxial angle (°)	Volume ($Å^3$)	Domain size (nm)	R_{wp} (%)
TNO-CB-CO_2	$Ti_2Nb_{10}O_{29}$	A12/*m*1	*a* = 15.64 *b* = 3.82 *c* = 20.52	β = 113.4	1124.1	55	3.4
TNO-OLC-CO_2	$Ti_2Nb_{10}O_{29}$	A12/*m*1	*a* = 15.62 *b* = 3.81 *c* = 20.52	β = 113.4	1122.4	63	3.7
TNO-CB-Air	$Ti_2Nb_{10}O_{29}$	A12/*m*1	*a* = 15.71 *b* = 3.85 *c* = 20.61	β = 113.4	1145.3	56	3.5
TNO-OLC-Air	$Ti_2Nb_{10}O_{29}$	A12/*m*1	*a* = 15.71 *b* = 3.85 *c* = 20.62	β = 113.4	1146.0	88	3.6

Table S3. Electrochemical performance comparison of titanium niobium oxides ($TiNb_2O_7$, and $Ti_2Nb_{10}O_{29}$). CNTs: carbon nanotubes. CF: carbon fiber. rGO: reduced graphene oxide. CNFs: carbon nanofibers. CC: carbon cloth. DEC: diethylene carbonate. DMC: dimethyl carbonate. EC: ethylene carbonate. EMC: ethyl methyl carbonate. PC: propylene carbonate. MSR: Mechanically-induced self-sustaining reaction.

Materials	Synthesis	Capacity at a low rate (mAh/g, A/g)	Capacity at a high rate (mAh/g, A/g)	Voltage range (V vs. Li/Li^+)	Capacity retention (%, cycle number)	Electrolyte	Reference
$TiNb_2O_7$/graphene hybrid	Solvothermal method	300, 0.03	150, 1.5	1.0-3.0	67, 300	1 M $LiPF_6$ in EC:DMC	[1]
Nano-$TiNb_2O_7$/CNTs	Direct hydrolysis method	300, 0.03	150, 4.5	0.8-3.0	97, 100	1 M $LiPF_6$ in EC:DMC:DEC	[2]
$TiNb_2O_7$/C nanoporous microspheres	Spray-drying method	393, 0.1	120, 3.6	1.0-2.6	75, 300	1 M $LiPF_6$ in EC:DEC	[3]
CF/$TiNb_2O_7$	Solvothermal method	250, 0.25	175, 1.75	1.0-2.5	88, 1000	1 M $LiPF_6$ in EC:DMC	[4]
rGO-$TiNb_2O_7$ microsphere	Solvothermal method	225, 0.23	25, 2.5	1.0-3.0	61, 500	1 M $LiPF_6$ in EC:EMC	[5]
$Ti_2Nb_{10}O_{29}$/C composite	Solid-state reaction	296, 0.25	150, 4.5	1.0-2.5	87, 100	1 M $LiPF_6$ in EC:DMC	[6]
$Ti_2Nb_{10}O_{29}$/rGO	Solid-state reaction, ball-milling	250, 0.03	100, 1	1.0-2.5	77, 50	1 M $LiPF_6$ in EC:DMC	[7]
$Ti_2Nb_{10}O_{29}$/carbon onion nanohybrid	Sol-gel method	290, 0.01	169, 2	1.0-2.8	76, 800	1 M $LiPF_6$ in EC:DMC	[8]
$Ti_2Nb_{10}O_{29}$/carbon hybrid fiber	Electrospinning	260, 0.025	180, 5	0.8-3.0	60, 500	1 M $LiPF_6$ in EC:DMC	[9]
$Ti_2Nb_{10}O_{29}$/C microsphere	Solvothermal method	276, 0.27	215, 6.4	1.0-2.5	89, 200	1 M $LiPF_6$ in EC:EMC:DEC	[10]
CNFs/$Ti_2Nb_{10}O_{29}$/CC	Electrophoretic deposition, solvothermal method	300, 0.03	200, 12	1.0-2.5	80, 1000	1 M $LiPF_6$ in EC:DEC	[11]
TNO-CB-CO_2	**MSR, CO_2 oxidation**	**272, 0.01** **304, 0.01**	**157, 1** **155, 1**	**1.0-2.5** **0.05-2.5**	**82, 500** **70, 500**	1 M $LiPF_6$ in EC:DMC	**This work**
TNO-OLC-CO_2	**MSR, CO_2 oxidation**	**253, 0.01** **350, 0.01**	**151, 1** **144, 1**	**1.0-2.5** **0.05-2.5**	**76, 500** **67, 500**	1 M $LiPF_6$ in EC:DMC	**This work**

Table S4. Results of the R_1, and R_2 obtained by fitting the data from **Fig. S8**.

Material	R_1 (Ω)	R_2(Ω)
TNO-CB-CO_2	16.2	168.8
TNO-OLC-CO_2	12.7	138.7
TNO-CB-Air	28.2	234.4
TNO-OLC-Air	7.3	184.4

References

[1] A. G. Ashish, P. Arunkumar, B. Babu, P. Manikandan, S. Sarang, M. M. Shaijumon, *Electrochim. Acta* **2015**, *176*, 285-292.
[2] C. Lin, L. Hu, C. Cheng, K. Sun, X. Guo, Q. Shao, J. Li, N. Wang, Z. Guo, *Electrochim. Acta* **2018**, *260*, 65-72.
[3] G. Zhu, Q. Li, Y. Zhao, R. Che, *ACS Appl. Mater. Interfaces* **2017**, *9*, 41258-41264.
[4] S. Shen, S. Deng, Y. Zhong, J. Wu, X. Wang, X. Xia, J. Tu, *Chin. Chem. Lett.* **2017**, *28*, 2219-2222.
[5] H. Noh, W. Choi, *J. Electrochem. Soc.* **2016**, *163*, A1042-A1049.
[6] G. Liu, B. Jin, R. Zhang, K. Bao, H. Xie, J. Guo, M. Wei, Q. Jiang, *Int. J. Hydrogen Energy* **2016**, *41*, 14807-14812.
[7] W. L. Wang, B.-Y. Oh, J.-Y. Park, H. Ki, J. Jang, G.-Y. Lee, H.-B. Gu, M.-H. Ham, *J. Power Sources* **2015**, *300*, 272-278.
[8] H. Shim, E. Lim, S. Fleischmann, A. Quade, A. Tolosa, V. Presser, *Sustainable Energy Fuels* **2019**, *3*, 1776-1789.
[9] A. Tolosa, S. Fleischmann, I. Grobelsek, A. Quade, E. Lim, V. Presser, *ChemSusChem* **2018**, *11*, 159-170.
[10] X. Liu, H. Wang, S. Zhang, G. Liu, H. Xie, J. Ma, *Electrochim. Acta* **2018**, *292*, 759-768.
[11] Y. Tang, S. Deng, S. Shi, L. Wu, G. Wang, G. Pan, S. Lin, X. Xia, *Electrochim. Acta* **2020**, *332*, 135433.